A Computational and Experimental Study of Deformations in a Draw Bead Welded Pipe

Model provides a better understanding of deflection behavior in draw bead welding

BY E. F. RYBICKI, R. B. STONESIFER, E. A. MERRICK AND J. R. HAUETER

ABSTRACT. Draw bead welding is a procedure used to align pipe ends for closure welds or to align bolted flange connections in piping systems. The draw bead weld has the appearance of a girth weld that is made partially around the circumference of the pipe. The nonsymmetrical nature of a draw bead weld causes the pipe to bend toward the side of the pipe where the weld metal is deposited.

Currently, data on deformations of draw bead welded pipes is limited, and there is a need for a computational model to better understand deformations resulting from draw bead welding. An exact model of the draw bead weld would require a three-dimensional analysis, which is too costly to run for the numerous cases required to study draw bead welding. This paper describes an approximate but efficient computational model that represents the welding parameters and geometric aspects of the draw bead weld. Laboratory data for the deflections of a draw bead welded pipe are also presented. Comparisons between the deflection data and values computed by the model show good agreement. The model is also used in a sensitivity study to evaluate the effects of the weld groove girth angle, the width of the draw bead weld groove, and the location of the weld pass on the amount of deflection experienced by the pipe.

Introduction

Draw bead welding is a procedure used to bend pipes during the construction of piping systems. Applications for this procedure are to correct misalignments of pipe ends in closure welds or flanged joints of piping systems. Figure 1 shows a specific example of the application of draw bead welding to a pipe. Generally, a draw bead weld is made part way around the circumference of a pipe, as shown in Figs. 1A and 1B. Referring to Fig. 1B, the weld groove is filled by a sequence of weld passes. Each pass starts near the 4 o'clock position and continues to the 12 o'clock position, then starts on the other side at the 8 o'clock position and stops at the 12 o'clock position. The effect of the procedure is to cause a bend in the pipe with the draw bead weld on the concave side of the pipe, as shown in Fig. 1A.

A principal advantage of applying the draw bead weld technique for improving alignment is that it reduces or eliminates the need for externally applied alignment forces, such as those from chain falls, which must then be supported by the joints. This advantage is important for cases where joint loads are critical. Such joints include bolted pipe flanges or a weldment to join a pipe to a nozzle, pump, valve or pressure vessel. The draw bead technique is, however, not without disadvantages. For example, the addition of a draw bead weld to the

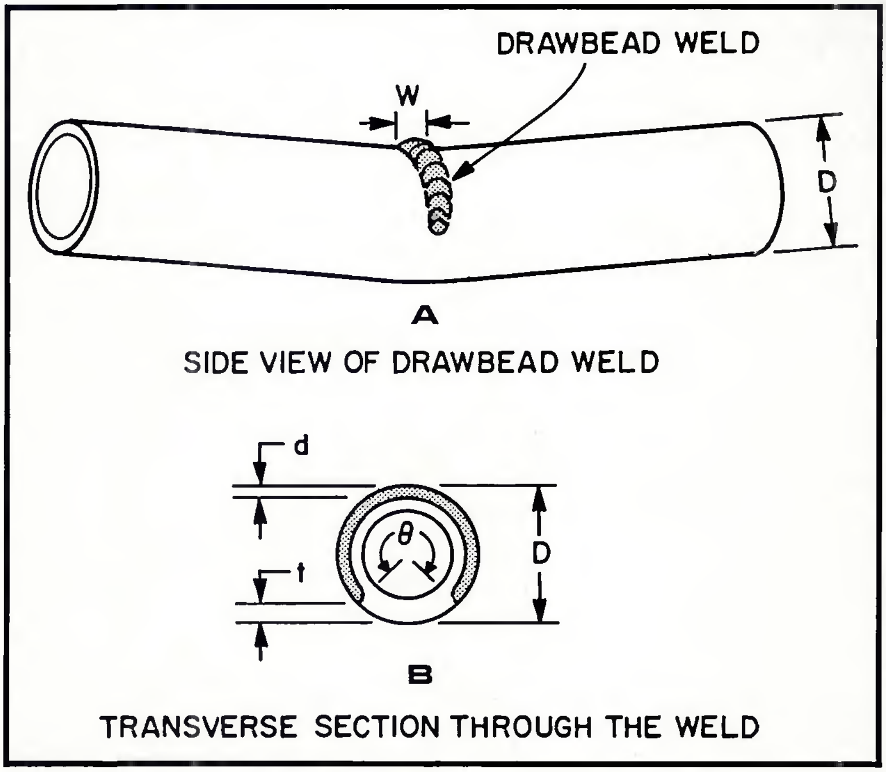

Fig. 1—Sketch of draw bead weld parameters for study

E. F. RYBICKI is Professor and Chairman of the Mechanical Engineering Department, University of Tulsa, Tulsa, Okla. R. B. STONESIFER is with Computational Mechanics, Inc., Julian, Pa. E. A. MERRICK and J. R. HAUETER are with the Tennessee Valley Authority, Knoxville, Tenn.

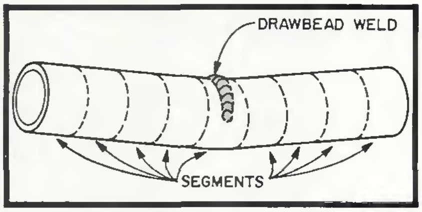

Fig. 2 — Illustration of segments for draw bead welded pipe model

piping system typically requires some drawing revisions, a possible additional weld examination, and the associated documentation additions. Another factor, which applies to all alignment procedures, but is worthy of note, is that if the pipe ends have been previously beveled, then realignment associated with the draw bead weld may require rebeveling.

The amount of deformation in the pipe is dependent upon the draw bead welding parameters utilized when applying the procedure. These parameters fall into two categories. One category can be defined as those associated with welding variables such as heat input and travel speed. The other category contains geometric parameters, such as pipe diameter, pipe thickness, and the depth, width and circumferential length of the weld groove.

While it is known that draw bead welding is affected by the welding process and joint design, the influence of welding variables and pipe geometry on the deformations of draw bead welds is presently not well understood. A better understanding of how to control deformations resulting from draw bead welding is needed to provide guidelines for developing a welding procedure to be used in field applications. This paper describes a combination of experiments and computational modeling studies selected to obtain an efficient method for predicting the behavior of draw bead welded pipes for a variety of draw bead welding conditions.

The problem of predicting residual deformations due to draw bead welding is complex because the weldment presents a three-dimensional geometry with temperature-dependent elastic-plastic, stress-strain behavior. A three-dimensional computational analysis, such as a finite element analysis for the draw bead welding procedure, would be costly for a single analysis and thus difficult to use to study a wide range of parameters. Thus, a more simplified analytical model is appropriate. The model should include the parameters of interest in the draw bead procedure.

The purpose of this paper is fourfold. The first is to present a simple computational model designed to represent the mechanics of draw bead welding. The second is to describe a draw bead weld experiment and the resulting deformation data. The third is to present comparisons between the deformations predicted by the computational model and the experimental data. These comparisons help to evaluate the ability of the computational model to represent the draw bead welding deformations. Finally, the model is used to study the effects of the weld groove length, width and depth on the resulting draw bead weld deformations.

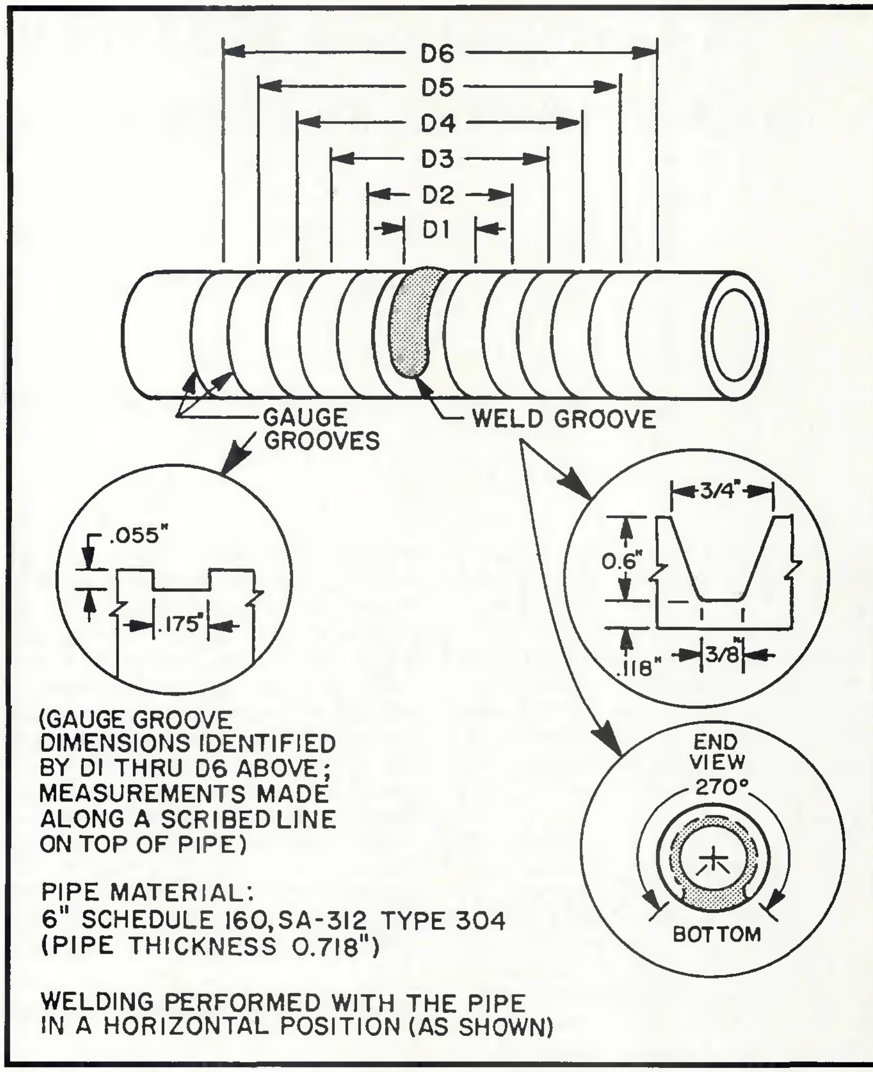

Fig. 3 — Draw bead mockup preparation

Computational Model

The computational model is developed with the goal of obtaining an efficient analytical tool to predict residual deformations for a range of draw bead welding conditions. The first step is to identify the characteristics to be included in the draw bead weld model. An illustration of a draw bead weld is shown in Fig. 1. Preparation for the draw bead weld generally consists of grinding a weld groove around part of the pipe circumference, as shown in Figs. 1A and 1B. The angle θ, shown in Fig. 1B, describes the circumferential length of the draw bead weld. The depth of the weld groove is denoted by d and the width of the weld is w. The pipe thickness and the outside diameter of the pipe are denoted by t and D, respectively.

As previously mentioned, the development of an efficient yet representative model is not straightforward because the geometry involved is three-dimensional and the stress-strain behavior is elastic-plastic and temperature dependent. To meet this challenge, some assumptions are required. Thus, it is important that the ability of the model to represent draw bead welding behavior be examined by comparisons with experimental deformation data.

The computational model for draw bead welding consists of two parts. The first part is a thermal analysis, which determines the transient thermal history of the welding process. The second part of the model is an elastic-plastic residual

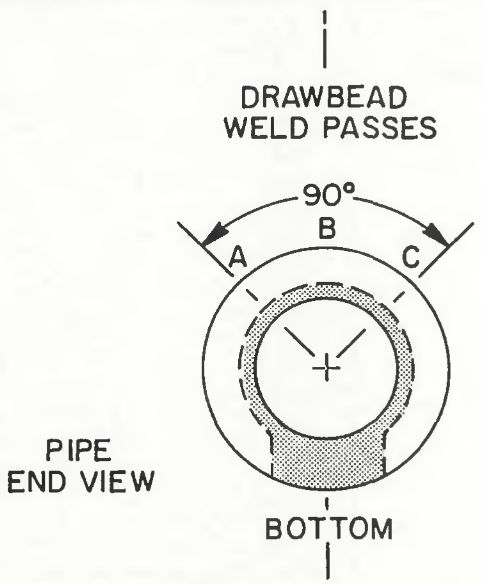

WELDING CONFINED TO THE UPPER 90° PORTION OF THE WELD GROOVE.
WELDING PROGRESSION WAS FROM POINT A TO POINT B, THEN FROM POINT C TO POINT B (ALTERNATING).

PASS	FILLER METAL	PROCESS	TYPICAL VALUES	
			CURRENT (AMPS)	SPEED (IPM)
1	ER308 3/32"	GT	70-85	1.5-2.0
2	ER308 3/32"	GT		
3	ER308 1/8"	GT	90-105	2.0-2.5
4	E308 1/8"	SM	90-115	3-4
5	E308 1/8"	SM		
6	E308 1/8"	SM		
7	E308 1/8"	SM		

Fig. 4—Step A of draw bead weld

deformation analysis. This component of the model evaluates deformations due to the thermal history. The draw bead welded pipe is represented by a series of connected segments, as shown in Fig. 2. A temperature distribution for each segment is evaluated, based on a modified version of the moving heat source temperature model developed in Ref. 1 and applied to girth welds in Refs. 2–6.

The temperature solution has been modified to represent the pipe geometry and weld groove dimensions, using two engineering assumptions. The first assumption is that the pipe can effectively be unwrapped to become a plate configuration. The second assumption is that the regions beyond the ends of the weld groove have thermal histories which are similar to the behavior on either side of the heat source path. The thermal model provides a temperature history for all points within each segment due to the draw bead weld. The temperature distributions are part of the input information for the elastic-plastic residual deformation model.

An important ingredient of the residual deformation model is the constitutive equations for elastic-plastic, temperature dependent behavior. The constitutive relations or the stress-strain-temperature equations incorporated in the model represent elastic-plastic behavior and include temperature dependent effects. The stress-strain behavior also contains strain hardening and represents the effect of loading, unloading and reloading, using the kinematic hardening assumption. The model assumes that the axial stress and strain behavior is primarily responsible for the residual bending deflections, and thus, the stress-strain relations are one-dimensional.

The temperature dependent stress-strain relations describe the material behavior at a point. To include the effect of the geometry of the draw bead welded pipe, the conditions of compatibility and equilibrium must be imposed. Compatibility is achieved by assuming compatible deformation modes. Equilibrium is achieved through the principle of virtual work (Ref. 7). For one-dimensional behavior, the virtual work principle can be expressed in equation form as

$$\int_V \sigma \, \delta\epsilon \, dv = \int_S \bar{t} \, \delta u \, dS \qquad (1)$$

where σ and ϵ are the axial stress and the axial strain within the volume of the pipe V; $\bar{t}$ is the prescribed axial traction on the end surfaces, S, of the pipe; and u is the axial displacement. While a complete derivation of the equations for the model is too lengthy to present here, some of the details are explained below. The deformations within each segment, shown in Fig. 2, are assumed to be of the form

$$u = (a + b\, r \cos \phi + c\, r \sin \phi)\, z \qquad (2)$$

where r and ϕ are the polar coordinates in the cylindrical coordinate system of each pipe segment and z is the axial coordinate. The coefficients a, b and c are the unknowns of the deformation field for segment i and are determined by the principle of virtual work. Because of the elastic-plastic nature of the problem, the stress-strain relations are in terms of incremental stresses and strains. The temperature history is applied as a sequence of temperature increments or load increments. Thus, Equation (1) is written in incremental form as

$$\int_V (\sigma_{l-1} + \Delta\sigma_l)\, \delta\epsilon_l \, dV = \int_S (\bar{t}_{l-1} + \Delta\bar{t}_l)\, \delta u_l \, dS \qquad (3)$$

where l denotes the current load increments, σ_{l-1} is the value of the axial stress at the end of the last load increment, $\Delta\sigma_l$ is the increment of stress for the present load increment, $\delta\epsilon_l$ is the virtual strain for the present increment, $\bar{t}_{l-1}$ is the value of the prescribed axial traction at the end of the last increment, $\Delta\bar{t}_l$ is the change in $\bar{t}$ during the present increment, and δu_l is the virtual axial displacement. The increment of the stress, $\Delta\sigma_l$, is related to the strain through the stress-strain equation. Substituting the incremental stress-strain relations and the incremental version of Equation (2) into Equation (3) and using standard variational methods (Ref. 7) results in a set of three equations with three unknowns for each pipe segment. It should be noted that the equations for each segment are not coupled to the equations for neighboring segments because of the planar nature of the assumed deformation mode represented by Equation (2).

The model can include the effect of applied axial loads and/or bending of the

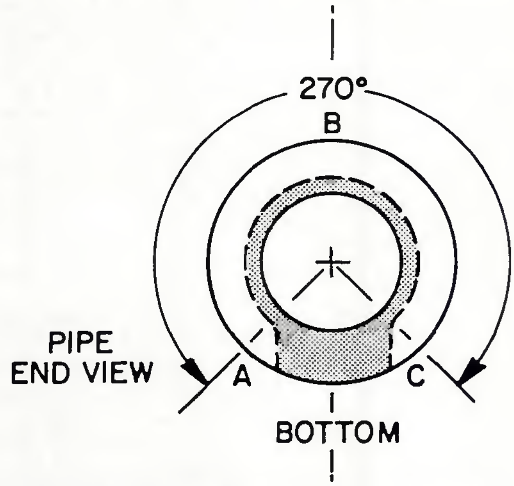

WELDING PERFORMED OVER THE FULL 270° OF THE WELD GROOVE.
WELDING PROGRESSION WAS FROM POINT A TO POINT B, THEN FROM POINT C TO POINT B (ALTERNATING FROM ONE SIDE TO THE OTHER).

PASS	FILLER METAL	PROCESS	TYPICAL VALUES CURRENT (AMPS)	SPEED (IPM)
8	ER308 1/8"	GT		
9	ER308 1/8"	GT		
10	ER308 1/8"	GT		
11	ER308 1/8"	GT	90-105	2.0-2.5
12	ER308 1/8"	GT		
13	ER308 1/8"	GT		
14	ER308 1/8"	GT		

Fig. 5 — Step B of draw bead weld

pipe. However, for the calculations presented here, axial forces and bending moments are not applied. The equations for the computational model were programmed on a microcomputer.

It was found that many of the ring segments shown in Fig. 2 experience elastic loading and elastic unloading because the temperature ranges are not high enough to produce plastic deformations. If no plasticity occurs in a segment, then that segment does not experience permanent deformations and does not have to be included in the analysis. For the case considered here, the plastic region was small enough so that one ring segment could be used to represent the axial length of the pipe experiencing plastic deformations. The length of this segment depends on the weld groove dimension w and the welding variables which determine the heat input and the temperature distributions. The length of the axial segment is generally greater than the pipe thickness. For the pipe considered here, the thickness is 0.718 in. (18.2 mm) and the segment size is 1.2 in. (30.5 mm).

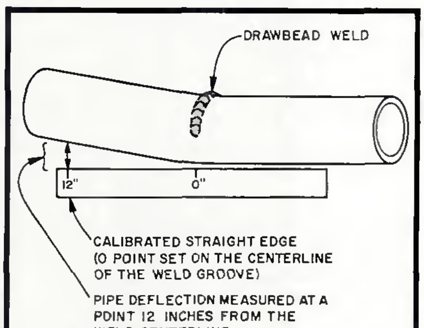

Fig. 6 — Measurement of pipe deflection data (generally, pipe deflection shown is greatly exaggerated)

Experimental Procedure

A 30 in. (0.76 m) segment of SA-312 Type 304 stainless steel pipe was selected for use in a draw bead mockup. The mockup was a 6 in. (152 mm) diameter schedule 160 pipe with a nominal section thickness of 0.718 in. (18.2 mm). The pipe was initially prepared for welding as shown in Fig. 3. The weld groove was manually prepared by grinding. A template was used to obtain dimensional accuracy. Deflection gauge grooves, shown in Fig. 3, were machined into the external pipe surface prior to preparation of the weld groove.

The sequence of welding was divided into two steps. In the first step, which is a 90 deg draw bead weld and is described in Fig. 4, the deposited weld metal was confined to the upper 90 deg of the groove, or 45 deg on either side of the top centerline. A total of seven weld passes were deposited in the groove, using two manual welding processes. The first three passes were deposited using the gas tungsten arc (GTA) process. The four subsequent passes were deposited with the shielded metal arc (SMA) process. The second welding step of the draw bead mockup was a 270 deg draw bead weld and is illustrated in Fig. 5. The 270 deg draw bead weld involved first the removal, by grinding, of all of the weld metal deposited by the 90 deg draw bead weld and then the completion of the full 270 deg groove weld, utilizing only the GTAW process. Seven passes were again deposited, and deflection data were taken at the location shown in Fig. 6.

Deflection data for each pass of the 270 deg weld were recorded and are shown in the third column of Table 1. All passes of the 270 deg weld, except number 11, produced a change in slope of 62 mils/ft. Pass 11 in Table 1 produced a change that was three times that of the other six passes. While the exact cause of this discrepancy is not known, the relatively large amount of deflection for pass 11 could in part be due to a longer cooling time for pass 11 (possibly deposited at the end of a working shift) than for the other six passes. Deflections were observed to increase when cooling time between passes was increased and also when the interpass temperature was decreased. In general, the weld passes of the draw bead mockup were allowed to cool until a bare hand could comfortably be placed on the pipe adjacent to the weld area.

Comparisons of Data and Computed Deflections

Comparisons of the computed values of deformations and the data are presented in Figs. 7 and 8 for passes 1 through 10. Note the excellent agreement between the model and the data for the 90 deg draw bead weld at pass 7 shown in Fig. 7 and the agreement for passes 8, 9 and 10 of the 270 deg draw bead weld shown in Fig. 8. Comparisons between the model deflections and the data are not made for passes 11 through 14 because, as noted in Table 1, the increase in deflection for pass 11 was unexplainably greater than the deflections for passes 8, 9 and 10. Thus, because the welding parameters and the conditions for pass 11 were most likely different than those for the other passes of the 270 deg draw bead weld, and because these parameters and conditions are undetermined, it was not possible to accurately represent pass 11 with the model for the purpose of comparison. However, if the change in deflection data for pass 11 was assumed to be the same as that for passes 8, 9, 10, 12, 13 and 14, the data would have been 622 mils/ft at the end of pass 14, as compared to 484 mils/ft predicted by the model for the same conditions.

Table 1—Table of Mockup Draw Bead Weld Deflection Results

Welding Step	Pass	Deflection[a] per Foot (mils/ft)	Change in[a] Deflection per Foot per Pass (mils/ft)
Initial	0	0	NA[b]
90 deg weld	1	NA	NA
90 deg weld	2	NA	NA
90 deg weld	3	NA	NA
90 deg weld	4	NA	NA
90 deg weld	5	NA	NA
90 deg weld	6	NA	NA
90 deg weld	7	188	NA
270 deg weld	8	250	62
270 deg weld	9	312	62
270 deg weld	10	374	62
270 deg weld	11	560	186[c]
270 deg weld	12	622	62
270 deg weld	13	684	62
270 deg weld	14	746	62

[a]Deflection measurements were made after the completion of the indicated pass.
[b]NA denotes that data were not available.
[c]No documentable reason was found for this threefold increase in deflection change for pass 11.

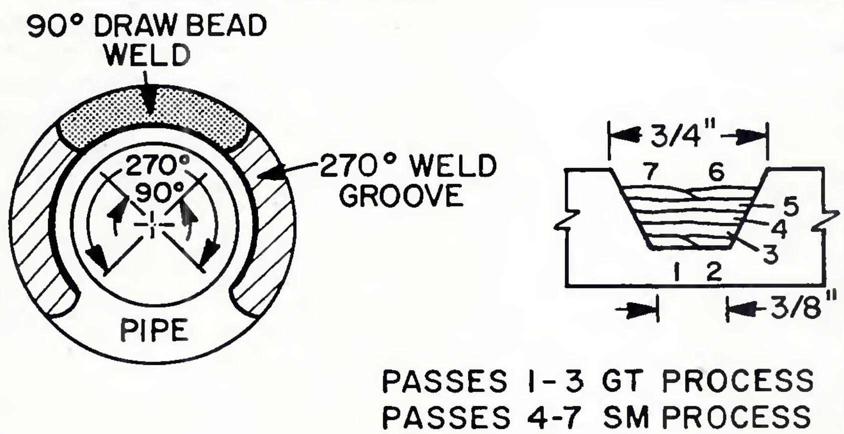

PASS	TYPE	δ, DEFLECTION PER FOOT (MILS/FT) MODEL	DATA
1	GT	30	NOT AVAILABLE
2	GT	52	NOT AVAILABLE
3	GT	74	NOT AVAILABLE
4	SM	113	NOT AVAILABLE
5	SM	139	NOT AVAILABLE
6	SM	163	NOT AVAILABLE
7	SM	185	188

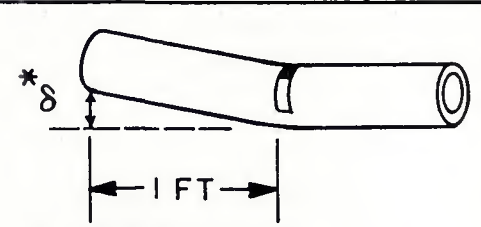

Fig. 7—Comparison of computer deflection with data for 90 deg draw bead weld

Effect of Weld Angle and Groove Width on Draw Bead Weld Deflections

Following the development of the computational model for draw bead welding and the comparisons with experimental deflection data, the model was utilized in a study to obtain a better understanding of the effect of changing the draw bead weld parameters on the final pipe deflections. The parameters selected were the girth angle G and the groove width w, shown in Fig. 9. The other geometric parameters of the draw bead weld shown in Fig. 9 were held at fixed values.

For this study, pipe dimensions for a 6 in. (152 mm) schedule 40 pipe were used. A heat input of 60 kJ/in. (236 kJ/m) and an arc speed of 3 ipm (76.2 mm/min) were selected. The depth of the weld groove was three quarters of the pipe thickness. Girth angles, G, in the range of 120-300 deg were considered. For this computation, two values for the width of the weld groove, w, shown in Fig. 9, were considered. One width was taken to be equal to the pipe thickness and the other was one half of the pipe thickness. Draw bead deflections are given in mils per foot per pass for a single pass. The results are shown in Fig. 10. The results show a peak deflection per foot per pass at a weld girth angle of approximately 180 deg.

The near optimum angle of a 180 deg weld is half of the circumference of the pipe. This result suggests that for these conditions, welding more than 180 deg begins to approach a girth weld and reduces the draw bead weld deflections.

While this part of the study points out a certain behavior for the 6 in. (152

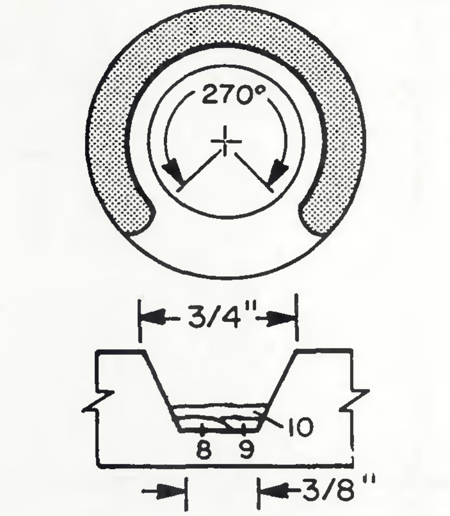

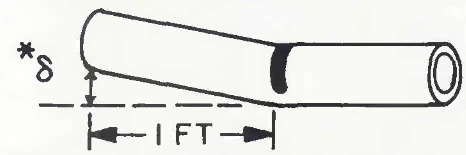

**DATA FROM TABLE 1 UP TO PASS 11, WHERE DATA WAS UNEXPLAINABLY LARGE.

	δ, DEFLECTION PER FOOT (MILS/FT)*	
PASS	MODEL	DATA**
7	185	188
8	256	250
9	294	312
10	330	374

Fig. 8 — Comparison of computed deflection with data for 270 deg draw bead weld for passes 8–10

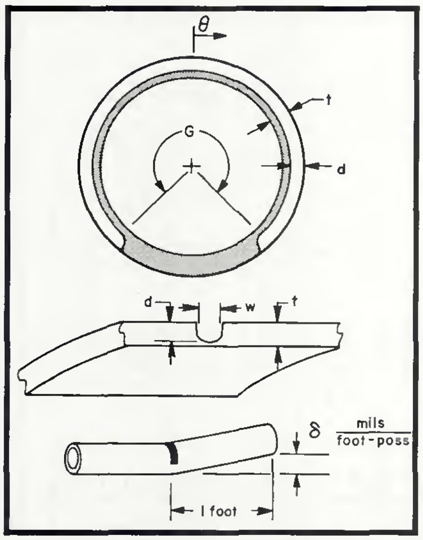

Fig. 9 — Notation used in the draw bead sensitivity study

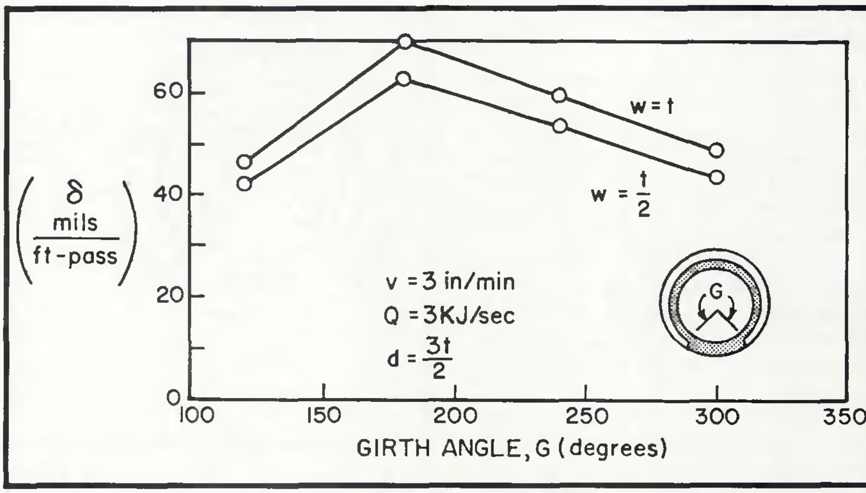

Fig. 10 — Sensitivity of per pass deflections (δ) to changes in girth angle and weld groove width for a 6 in., schedule 40, 304 stainless steel pipe

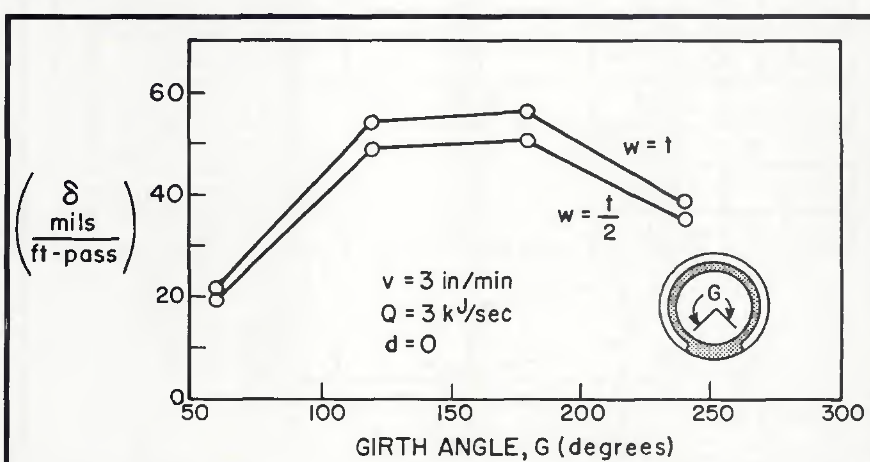

Fig. 11 — Sensitivity of per pass deflection (δ) to changes in girth angle and pass width of a 6 in., schedule 40, 304 stainless steel pipe. (Weld pass placed on the outer surface of the pipe)

mm) schedule 40 pipe, the results should not be generalized for all pipe sizes, schedules and welding conditions. Rather, the draw bead process involves many parameters which interact in a complex manner to produce the resulting deformations. For example, it was found that the distance of the weld pass from the pipe inner surface has an effect on the resulting deformations. To illustrate this behavior, several cases were modeled. Using the same heat input and arc speeds used in the previous cases, the weld pass was placed on the surface of the pipe so that the weld groove depth, d, shown in Fig. 9, was zero. The effect of weld girth angle for these conditions is shown in Fig. 11 for an angular range of 60–240 deg. When compared with Fig. 10, the results in Fig. 11 show a decreasing trend in deflections for increasing weld angles between 180 and 240 deg. Comparisons of Figs. 10 and 11 also illustrate the interaction of the draw bead weld parameters on the final deflection and indicate that extrapolation to other cases should not be made from the limited database presented here.

Conclusions and Recommendations

A combined experimental and computational modeling study of the draw bead welding process was presented. An efficient computational model was developed for the complex draw bead welding conditions. The computational model includes important characteristics of the draw bead weld. The model represents elastic-plastic, temperature dependent, constitutive behavior and the important geometric parameters describing the draw bead weld configuration.

Comparisons between computed values of weld deflections and laboratory data taken for a draw bead welded pipe showed good agreement for passes 1 through 10. The uncertainty of the data for pass 11 made further comparisons questionable. However, estimates of the data beyond pass 11 indicated a growing difference between the measured deflections and the computer values. Concerning the margin of difference between the deflection data and the values predicted by the model, the model is viewed primarily as a simple tool for gaining a better understanding of the various draw bead weld parameters, rather than a means to accurately predict the behavior of a given weld. It should be noted that any changes in current draw bead weld procedures will have to be developed and qualified and will not be based only on the results of a model. Draw bead welds in the field will most likely have to be monitored to prevent over or under drawing.

The model was then used to examine the effects of selected draw bead weld parameters on the final pipe deformation. The results for a 6 in. (152.4 mm) schedule 40 pipe showed two important features. One feature was that a specific girth angle could be found to produce maximum deflections for specific sets of welding conditions. The second characteristic was that the draw bead weld deflections for a single pass showed different amounts of deflection, depending upon where the pass was located in the weld groove. Thus, the results suggest that the draw bead weld deflection behavior is dependent upon the draw bead geometric parameters and welding variables in a complex manner. Also, because both the variables related to the welding procedure and the geometric variables have an effect on the results of draw bead welding, and in keeping with the general industry methods and the procedures of Section IX of the Code, autogenous welding is not recommended for use on draw beads.

While the ability of the computational model to predict measured deflections is very encouraging and the sensitivity studies show interesting trends, the results and the limited database for the cases considered here need to be expanded before extrapolations to other pipe sizes and welding conditions can be made. However, the model appears to have the potential to be an effective tool for obtaining a better understanding of what is happening when draw bead welds are made and for developing new draw bead weld procedures for a range of pipe sizes and welding conditions.

References

1. Rosenthal, D. 1941. Mathematical theory of heat distribution during welding and cutting. *Welding Journal* 20(5):220-s to 234-s.
2. Rybicki, E. F., Schmueser, D. W., Stonesifer, R. B., Groom, J. J., and Mishler, H. W. 1978. A finite element model for residual stresses and deflections in girth-butt welded pipes. *Journal of Pressure Vessel Technology* 100(8):256-262.
3. Rybicki, E. F., and Stonesifer, R. B. 1979. Computation of residual stresses due to multipass welds in piping systems. *Journal of Pressure Vessel Technology* 101(5):149-153.
4. Rybicki, E. F., and Stonesifer, R. B. 1980. An analysis procedure for predicting weld repair residual stresses in thick-walled vessels. *Journal of Pressure Vessel Technology* 102(8):323-331.
5. Rybicki, E. F., McGuire, P. A., Merrick, E., and Wert, J. 1982. The effect of pipe thickness on residual stresses due to girth welds. *Journal of Pressure Vessel Technology* 104(8):204-209.
6. Rybicki, E. F., and McGuire, P. A. 1981. A computational model for improving weld residual stresses in small diameter pipes by induction heating. *Journal of Pressure Vessel Technology* 103(8):294-299.
7. Dym, C. L., and Shames, I. H. 1973. *Solid Mechanics: A Variational Approach*. McGraw-Hill Book Co., New York, N.Y.